Biomedical Signal Processing and Control 78 (2022) 103851

Contents lists available at ScienceDirect

Biomedical Signal Processing and Control

journal homepage: www.elsevier.com/locate/bspc

A novel computational model for cerebral blood flow rate control mechanisms to evaluate physiological cases

Selim Bozkurt [a,*], A. Volkan Yilmaz [b], Kaushiki Bakaya [c], Aniket Bharadwaj [d], Koray K. Safak [b]

[a] Ulster University, School of Engineering, Shore Rd, Newtownabbey BT37 0QB, UK
[b] Yeditepe University, Department of Mechanical Engineering, Kayisdagi, Inonu Mah, Kayisdagi Cd., 34755 Istanbul, Turkey
[c] University College London, School of Medicine, 74 Huntley St, London WC1E 6DE, UK
[d] Cambridge University Hospital, Department of Medicine, Hills Rd, Cambridge CB2 0QQ, UK

ARTICLE INFO

Keywords:
Cerebral blood flow rate regulation
Cardiovascular system
Cerebral circulation
Numerical modelling
Physiological control systems

ABSTRACT

In this study, a new numerical model simulating interaction among static cerebral autoregulation, cerebrovascular CO_2 and O_2 reactivities and systemic peripheral resistance regulation was developed and integrated into a cardiovascular system model including heart chambers, systemic and pulmonary circulations, and cerebral circulation with Circle of Willis. Simulations were performed to evaluate cerebral blood flow in a healthy condition, effect of altered static cerebral autoregulation in heart failure, effect of impaired static cerebral autoregulation in malignant hypertension, effects of arterial CO_2 and O_2 pressures in hypercapnia, hypocapnia and hypoxemia on cerebral blood flow. Also, sensitivity analysis was performed to assess influence of arterial CO_2 and O_2 pressure, aortic pressure set point in the cerebral flow autoregulatory function, systemic peripheral resistance, left ventricular active and passive properties on the cerebral blood flow rate. There was a high and positive correlation between cerebral blood flow rate and arterial CO_2 pressure whereas left ventricular contractility influenced cerebral blood flow rate slightly. Cerebral blood flow rate in the healthy condition, heart failure, malignant hypertension, hypercapnia, hypocapnia and hypoxemia was 721 mL/min, 606 mL/min, 1313 mL/min, 950 mL/min, 504 mL/min and 972 mL/min, respectively. Simulation results and sensitivity analysis showed that the new numerical model can be used to evaluate cerebral blood flow in various physiological cases.

1. Introduction

Cerebral blood flow rate is regulated by highly complex and interacting mechanisms such as autoregulatory function, metabolic, chemical or neurogenic mechanisms to keep the brain functioning properly under normal conditions [1,2]. Metabolic control of cerebral blood flow rate implies the coupling between cerebral flow, cerebral metabolism and cerebral function [3]. Chemical control of cerebral blood flow rate implies response of the cerebral blood flow rate to the arterial gases such as CO_2 [4]. Neurogenic cerebral flow rate control mechanisms include role of perivascular nerves in regulating the cerebral blood flow [4].

Cerebral flow rate autoregulation mechanisms are affected by the health problems such as ischemia, congestive heart failure or chronic hypertension [5–7] and some of these mechanisms have been modelled to simulate healthy conditions and clinical cases. For instance, Ursino modelled human intracranial hydrodynamics and simulated clinical scenarios [8]. Piechnik et al., [9] modelled relationship between cerebral blood volume and flow rate for CO_2 manipulation whereas interaction between the CO_2 reactivity and intracranial pressure is modelled by Ursino and Lodi [10]. The latter model was also extended to simulate interaction between the cerebral flow rate autoregulatory function, cerebrovascular CO_2 reactivity and intracranial pressure [11]. Aoi et al., [12] optimised a model simulating the cerebral flow rate autoregulatory function using patient data. Banaji et al., [13] combined simplified models of circulatory system, brain metabolic biochemistry, and a model of the functioning of vascular smooth muscle to simulate cerebral blood flow rate control. Payne et al., [14] modelled effects of cerebral flow autoregulation and CO_2 reactivity on cerebral oxygen transport. Spronck et al., [15] developed a lumped parameter model of cerebral blood flow control combining cerebral autoregulation and neurovascular coupling. Mahdi et al., developed a model simulating interaction between arterial between baroreflex control and cerebral flow autoregulation [16]. Czosnyka et al., [17] modelled interactions among the pressure, flow rate and cerebral blood volume and

* Corresponding author.
E-mail address: s.bozkurt1@ulster.ac.uk (S. Bozkurt).

https://doi.org/10.1016/j.bspc.2022.103851
Received 24 April 2022; Received in revised form 27 May 2022; Accepted 4 June 2022
Available online 14 June 2022

cerebrospinal fluid using a lumped parameter model for cerebral circulation. Piechnik et al., [18] studied the asymmetry of hemispheric blood flow rate in response to simulated changes in arterial blood pressure and carbon dioxide concentration using a lumped parameter model.

Clinical cases have been also evaluated using numerical and experimental models for the cerebral blood flow rate regulation mechanisms. For instance, Duffin et al., [19] developed a mathematical model of cerebral blood flow control in anaemia and hypoxia. Liu et al., [20] evaluated cerebral autoregulation indices from modelling perspective. Bozkurt evaluated effect of cerebral flow rate autoregulatory function on cerebral flow rate during left ventricular assist device support utilising numerical simulations [21]. Furthermore, time and frequency domain methods have been utilised to analyse and model cerebral autoregulation in clinical cases [22]. Although different models and modelling approaches have been used to simulate cerebral blood flow rate autoregulation only a few studies aim to simulate physiological cases affecting the cerebral autoregulation as presented in [23]. Numerical models simulating cerebral blood flow rate regulation mechanisms and capable of describing altered cerebral circulation physiology in clinical cases such as heart failure or hypertension can also be utilised to study treatments methods as well.

In this study, a new numerical model simulating static cerebral autoregulatory function, cerebrovascular CO_2 and O_2 reactivities and arterial baroreflex regulation was developed and used to evaluate effect of physiological cases such as heart failure, impaired cerebral autoregulation due to malignant hypertension, hyper and hypoventilation and hypoxemia on cerebral blood flow rate. The developed numerical model simulates altered cerebral flow rate autoregulation in heart failure with reduced ejection fraction whilst a detailed cerebral circulation model includes compartments such middle cerebral arteries allowing to compare clinical data to the simulation results.

2. Methods

Numerical model used in this study includes cerebral flow rate autoregulatory functions, CO_2 and O_2 cerebrovascular reactivity and a cardiovascular system model. Cardiovascular system model includes compartments simulating heart chambers and heart valves, systemic and pulmonary circulations, cerebral circulation, systemic arteriolar resistance regulation mechanism.

Simulations were performed using Matlab Simulink R2021b. The set of equations was solved using the ode15s solver. The maximum step size was 5e-4 s, relative tolerance was set to 5e-4. The heart rate was kept at 75 bpm for all the conditions in the numerical simulations. The abbreviations used in the equations and figures are given in Table 1. The parameter values used in the cardiovascular system model and cerebral flow rate regulation mechanisms for each physiological scenario are given in Supplementary Material 1 and the numerical models together with the description of each model are given in Supplementary Material 2.

2.1. Cerebral flow rate control mechanisms

In this study, cerebrovascular CO_2 and O_2 reactivities and static cerebral autoregulatory function were modelled. These mechanisms control the resistance of pial circulation (R_{pc}) to regulate the cerebral flow rate in the numerical model.

2.1.1. Cerebrovascular CO_2 reactivity

Change in arterial CO_2 pressure affects the cerebral flow rate significantly. Radii of the cerebral arteries increase as response to increasing arterial CO_2 pressure and cerebral blood flow rate increases with the increasing arterial CO_2 pressure to remove the CO_2 from brain tissue [24]. An exponential model (Eq. (1)) which utilises arterial CO_2 pressure ($p_{a,CO2}$) was developed to regulate resistance of the pial circulation ($R_{pc,CO2}$) using the data for the change in total cerebral blood flow rate with respect to arterial CO_2 pressure given in [11,25,26]. The numerical model in [21] was used to simulate cerebral blood flow rate change as given [11,25,26] to generate a data set for the arterial CO_2 pressure ($p_{a,CO2}$) and resistance of the pial circulation ($R_{pc,CO2}$). The cerebrovascular CO_2 reactivity model was developed using the generated data in Curve Fitting Toolbox in Matlab R2021b. Data used to develop cerebrovascular CO_2 reactivity are given in Table 2.

$$R_{pc,CO_2} = R_{pc,set} * a_1 * e^{a_2 * p_{a,CO2}} \quad (1)$$

Here, $R_{pc,set}$ represents set point for the resistance of the pial circulation at 40 mmHg arterial CO_2 pressure ($p_{a,CO2}$) and a_1 and a_2 are coefficients in the model.

2.1.2. Cerebrovascular O_2 reactivity

Cerebral blood flow rate is not very sensitive to the changes in

Table 1
Abbreviations used in the equations and figures.

Nomenclature		roa	right ophthalmic artery
p	pressure	loa	left ophthalmic artery
V	volume	ba	basilar artery
Q	flow rate	pca	posterior cerebral arteries
t	time	rpca	right posterior cerebral artery
R	resistance	lpca	left posterior cerebral artery
L	inertance	rpcoa	right posterior communicating artery
C	compliance	lpcoa	left posterior communicating artery
AV	aortic valve	rsca	right superior cerebellar artery
MV	mitral valve	lsca	left superior cerebellar artery
PV	pulmonary valve	racha	right anterior choroidal artery
TV	tricuspid valve	lacha	left anterior choroidal artery
EF	ejection fraction	rmca	right middle cerebral artery
MAP	mean arterial pressure	lmca	left middle cerebral artery
CO	cardiac output	mca	middle cerebral artery
S	sensitivity	raca	right anterior cerebral artery
Subscripts		laca	left anterior cerebral artery
la	left atrium	acoa	anterior communicating artery
lv	left ventricle	pc	pial circulation
ra	right atrium	cc	cerebral capillaries
rv	right ventricle	vc	cerebral veins
ao	aorta	es	end systolic
aa	aortic arch	cbf	cerebral blood flow
ars	systemic arterioles	set	set point
cs	systemic capillaries	m	mean
vs	systemic veins	n	normalised
ap	pulmonary arteries	CO_2	carbon dioxide
arp	pulmonary arterioles	O_2	oxygen
vp	pulmonary veins	p_{CO2}	carbon dioxide pressure
rica	right internal carotid artery	p_{O2}	oxygen pressure
lica	left internal carotid artery	0	zero value, initial
rva	right vertebral artery	1	segment one
lva	left vertebral artery	2	segment two

Table 2
Arterial CO_2 pressures, cerebral flow rates and pial circulation resistances used to develop cerebrovascular CO_2 reactivity model.

Arterial CO_2 Pressure [mmHg]	Cerebral Flow Rate [mL/s]	Pial Circulation Resistance [mmHg s/mL]
100	24.08	0.23
90	22.87	0.41
80	21.65	0.61
70	19.87	0.95
60	18.13	1.34
50	15.06	2.25
40	12.03	3.60
30	7.87	7.15
20	6.02	10.30

arterial O_2 pressure. Cerebral blood flow rate remains relatively constant for the arterial O_2 pressures higher than 50 mmHg [27]. A two-term exponential model (Eq. (2)) utilising arterial O_2 pressure ($p_{a,O2}$) was developed to regulate resistance of the pial circulation ($R_{pc,O2}$) using the data for the change in total cerebral blood flow rate with respect to arterial O_2 pressure reported in [28]. The numerical model in [21] was used to simulate cerebral blood flow rate change as given [28] to generate a data set for the arterial O_2 pressure ($p_{a,O2}$) and resistance of the pial circulation ($R_{pc,O2}$). The cerebrovascular O_2 reactivity model was developed using the generated data in Curve Fitting Toolbox in Matlab R2021b. Data used to develop cerebrovascular O_2 reactivity are given in Table 3.

$$R_{pc,O_2} = R_{pc,set}\left(b_1 * e^{b_2 * p_{a,O2}} + b_3 * e^{b_4 * p_{a,O2}}\right) \tag{2}$$

Here, $R_{pc,set}$ represents set point for the resistance of the pial circulation at 100 mmHg arterial O_2 pressure ($p_{a,O2}$) and b_1, b_2, b_3 and b_4 are coefficients in the model.

2.1.3. Static cerebral flow rate autoregulatory function

Static cerebral flow rate autoregulatory function maintains the average cerebral blood flow rate at a relatively constant value between 60 mmHg and 120 mmHg mean arterial blood pressure [29]. A model was adopted from [21] to regulate resistance of the pial circulation ($R_{pc,ao}$) with respect to mean arterial pressure ($p_{ao,m}$) in the simulations.

$$\Delta R_{pc,pao} = \left|S_{Rpc,pao}(p_{ao,cbf,set} - p_{ao,m})R_{pc,set}\right| \tag{3}$$

$$R_{pc,pao} = \begin{cases} R_{pc,pao} - \Delta R_{pc,pao} & p_{ao,m} \geqslant p_{ao,cbf,set} \\ R_{pc,pao} + \Delta R_{pc,pao} & p_{ao,m} < p_{ao,cbf,set} \end{cases} \tag{4}$$

Here, $S_{Rpc,ao}$, $\Delta R_{pc,ao}$, $R_{pc,set}$ and $p_{ao,cbf,set}$ represent sensitivity of the pial circulation resistance, change in the pial circulation resistance, pial circulation resistance at the aortic pressure set point and aortic pressure set point in the cerebral flow autoregulatory function.

2.1.4. Interaction of the cerebral flow rate regulation mechanisms

Interaction among the cerebrovascular CO_2 and O_2 reactivities and the static cerebral autoregulatory function was modelled using normalised resistance of the pial circulation ($R_{pc,pCO2}$, $R_{pc,pO2}$, $R_{pc,pao,m}$) for each mechanism as given below.

$$R_{pc} = R_{pc,set} * R_{pc,p_{CO2,n}} * R_{pc,p_{O2,n}} * R_{pc,p_{ao,n}} \tag{5}$$

Here, R_{pc} and $R_{pc,set}$ represent resistance of the pial circulation and set point of the pial circulation resistance for healthy condition. Normalised resistance of the pial circulation for each mechanism are simulated by as given below.

$$R_{pc,p_{CO2,n}} = R_{pc,p_{CO2}}/R_{pc,set} \tag{6}$$

$$R_{pc,p_{O2,n}} = R_{pc,p_{O2}}/R_{pc,set} \tag{7}$$

$$R_{pc,p_{ao,n}} = R_{pc,p_{ao}}/R_{pc,set} \tag{8}$$

Table 3
Arterial O_2 pressures, cerebral flow rates and pial circulation resistances used to develop O_2 reactivity model.

Arterial O_2 Pressure [mmHg]	Cerebral Flow Rate [mL/s]	Pial Circulation Resistance [mmHg s/mL]
35	23.82	0.27
40	18.64	1.22
50	14.43	2.48
60	12.99	3.10
70	12.50	3.35
80	12	3.60
90	12	3.60
100	12	3.60
110	12	3.60
120	12	3.60
130	12	3.60
140	12	3.60
150	12	3.60
160	12	3.60
170	12	3.60
180	12	3.60

2.2. Cardiovascular system model

Left and right ventricular functions were described by modelling the relationship between ventricular pressure and volume variation over a cardiac cycle. Left ventricular pressure (p_{lv}) was modelled to simulate active and passive contractions during systolic and diastolic phases as given below.

$$p_{lv} = p_{lv,a} + p_{lv,b} \tag{9}$$

$$p_{lv,a}(t) = E_{es,lv}\left(V_{lv} - V_{lv,0}\right)f_{act,lv}(t) \tag{10}$$

$$p_{lv,p} = A\left(e^{B\left(V_{lv} - V_{lv,0}\right)} - 1\right) \tag{11}$$

Here, $p_{lv.a}$ and $p_{lv,p}$ are the active and passive components of the left ventricular pressure (p_{lv}). $E_{es,lv}$ is the left ventricular end-systolic elastance, V_{lv} and $V_{lv,0}$ left ventricular volume and zero-pressure volume in the left ventricle. $f_{act,lv}$ is the left ventricular activation function. A and B are coefficients used in the left ventricular passive pressure model. Left ventricular volume (V_{lv}) was modelled using the left ventricular radius (r_{lv}), long axis length (l_{lv}) and a parameter (K_{lv}) which includes effects of the contraction in the long axis. Change of the left ventricular radius (r_{lv}) was described using the flow rates through the aortic and mitral valves (Q_{av}, Q_{mv}), left ventricular volume (V_{lv}), long axis length (l_{lv}) and the coefficient K_{lv}.

$$V_{lv} = \frac{2}{3}\pi K_{lv} r_{lv}^2 l_{lv} \tag{12}$$

$$\frac{dr_{lv}}{dt} = \frac{3(Q_{mv} - Q_{av})}{4\pi K_{lv} l_{lv}}\left(\frac{3V_{lv}}{2\pi K_{lv} l_{lv}}\right)^{-1/2} \tag{13}$$

The activation function ($f_{act,lv}$) was described using instantaneous time (t), the durations of active contraction (T_1) and relaxation (T_2) phases and the duration of a cardiac cycle (T) [30].

$$f_{act,lv}(t) = \begin{cases} \dfrac{1 - \cos((t/T_1)\pi)}{2} & 0 \leqslant t < T_1 \\ \dfrac{1 + \cos((t - T_1)/(T_2 - T_1)\pi)}{2} & T_1 \leqslant t < T_2 \\ 0 & T_2 \leqslant t < T \end{cases} \tag{14}$$

Right ventricular pressure and volume over a cardiac cycle were modelled in a similar way using different parameter values. Detailed information about modelling of the left and right ventricular functions can be found in [31].

Left and right atrial functions were modelled using atrial elastances. Left atrial pressure (p_{la}) was described using left atrial volume (V_{la}), zero-pressure volume ($V_{la,0}$) and left atrial elastance (Ela).

$$p_{la}(t) = E_{la}(t)\left(V_{la} - V_{la,0}\right) \tag{15}$$

Left atrial volume (V_{la}) was described using the left atrial radius (r_{la}), long axis length (l_{la}) and a scaling parameter (K_{la}). Change of the left atrial radius (r_{la}) was described using the flow rates through the mitral valve and pulmonary vein (Q_{mv}, Q_{vp}), left atrial volume, long axis length and K_{la} [31].

$$V_{la} = \frac{2}{3}\pi K_{la} r_{la}^2 l_{la} \tag{16}$$

$$\frac{dr_{la}}{dt} = \frac{3\left(Q_{pv} - Q_{mv}\right)}{4\pi K_{la} l_{la}} \left(\frac{3V_{la}}{2\pi K_{la} l_{la}}\right)^{-1/2} \tag{17}$$

Left atrial elastance function was described using left atrial minimal and maximal elastances ($E_{min,la}$, $E_{max,la}$) and left atrial activation function ($f_{act,la}$). Left atrial activation function ($f_{act,la}$) was described using time (t) and atrial activation time instant (T_a) [30] as given below.

$$E_{la}(t) = E_{\min,la} + 0.5\left(E_{\max,la} - E_{\min,la}\right) f_{act,la}(t - D) \tag{18}$$

$$f_{act,la}(t) = \begin{cases} 0 & 0 \leqslant t < T_a \\ 1 - \cos\left(2\pi \dfrac{t - T_a}{T - T_a}\right) & T_a \leqslant t < T \end{cases} \tag{19}$$

The right ventricular pressure and volume signals were modelled in a similar way to the left ventricular pressure and volume signals using different parameter values. Detailed information about the models used to describe atrial ventricular functions can be found in [31].

Heart valves were modelled as ideal diodes allowing one-way blood flow. Circulatory system was modelled using resistance (R), inertance (L) and compliance (C) elements. Change of aortic pressure (dp_{ao}/dt) and flow rate (dQ_{ao}/dt) with respect to time are given below.

$$\frac{dp_{ao}}{dt} = \frac{Q_{av} - Q_{ao}}{C_{ao}} \tag{20}$$

$$\frac{dQ_{ao}}{dt} = \frac{p_{ao} - p_{aa} - Q_{ao}R_{ao}}{L_{ao}} \tag{21}$$

Here, Q_{av} is the aortic valve blood flow rate, C_{ao} is the aortic compliance, p_{aa} is the pressure in the aortic arch, R_{ao} and L_{ao} are the aortic resistance and inertance. In the cardiovascular system model, systemic circulation includes aorta, aortic arch, systemic arterioles,

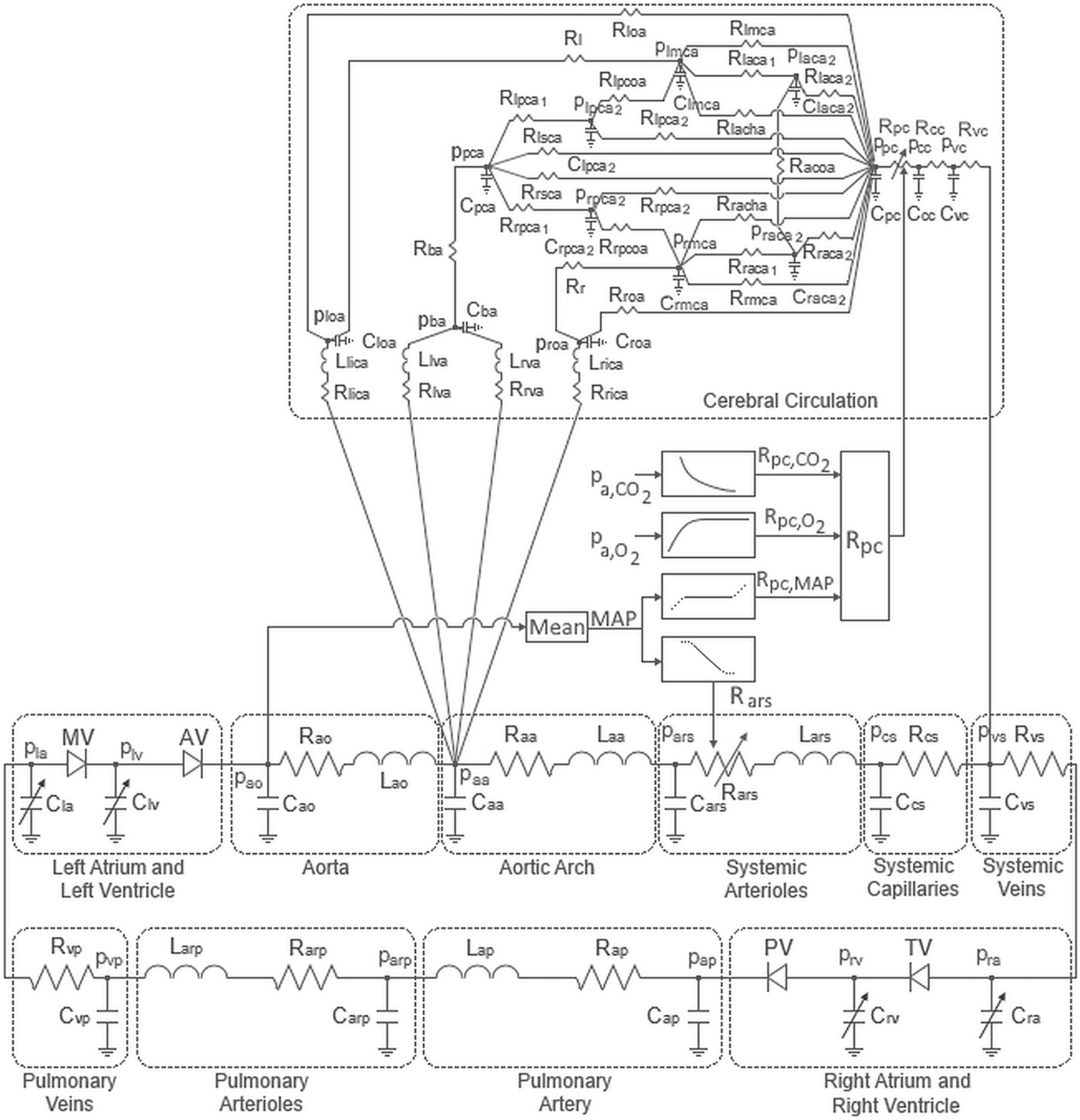

Fig. 1. Electric analogue of the cardiovascular system model and the block diagram for the cerebral flow rate regulatory mechanisms.

capillaries and veins, pulmonary circulation includes pulmonary arteries, peripheral pulmonary circulation and pulmonary veins. Cerebral circulation includes left and right internal carotid arteries, left and right vertebral arteries, basilar artery, left and right superior cerebellar arteries, left and right anterior choroidal arteries, left and right ophthalmic arteries, left and right middle arteries, left and right posterior cerebral arteries, left and right posterior communicating arteries, left and right anterior cerebral arteries, and the anterior communicating artery, pial circulation, cerebral capillaries and cerebral veins. Pressure and blood flow rate in these compartments were simulated in a similar way to aorta (Eq. (20) and (21)) using different parameter values. All the blood vessels on the left and right sections in the cerebral circulation are assumed to be identical. Because blood flow is distributed uniformly in Circle of Willis and does not vary considerably in each section on the left and right sides unless there are significant anatomical variations or anomalies in the structure of the cerebral arteries [32].

Systemic arteriolar resistance (R_{ars}) was regulated using mean aortic pressure ($p_{ao,m}$) in the cardiovascular system model as described in [33].

$$\Delta R_{ars} = \left| S_{Rars}(p_{ao,ars,set} - p_{ao,m}) R_{ars,set} \right| \tag{22}$$

$$R_{ars} = \begin{cases} R_{ars} - \Delta R_{ars} & p_{ao,m} \geq p_{ao,ars,set} \\ R_{ars} + \Delta R_{ars} & p_{ao,m} < p_{ao,ars,set} \end{cases} \tag{23}$$

Here, S_{Rars}, ΔR_{ars}, $R_{ars,set}$ and $p_{ao,ars,set}$ represent sensitivity of the systemic arteriolar resistance, change in the systemic arteriolar resistance, systemic arteriolar resistance at the aortic pressure set point and aortic pressure set point in the systemic arteriolar resistance control. Electric-analogue diagram of the heart and circulatory system model and block diagram of the blood flow rate regulatory mechanisms are given in Fig. 1.

2.3. Physiological scenarios

Computational simulations were performed to evaluate following clinical scenarios: cerebral flow rate autoregulatory mechanisms with healthy cardiac function and heart failure with reduced ejection fraction, impaired cerebral flow rate autoregulatory function due to malignant hypertension, hypercapnia, hypocapnia and hypoxemia.

2.3.1. Normal cardiac function and cerebral flow rate autoregulation mechanisms

Normal cardiovascular system physiology and cerebral flow rate regulatory mechanisms were simulated using the setpoints for left ventricular systolic elastance, parameter A, left ventricular zero pressure volume ($E_{es,lv}$ = 2.5 mmHg/mL, A = 1 mmHg, $V_{lv,0}$ = 15 mL) [31], arterial CO_2 and O_2 pressures ($p_{a,CO2}$ = 40 mmHg, $p_{a,O2}$ = 100 mmHg) [34,35] and the aortic pressure set point in the cerebral flow autoregulatory function ($p_{ao,cbf,set}$ = 93 mmHg) [36] which yield cardiac output, ejection fraction and mean cerebral flow rate over a cardiac cycle within a physiological range for healthy conditions.

2.3.2. Heart failure with reduced ejection fraction

Cardiac function in heart failure with reduced ejection fraction was simulated reducing the left ventricular systolic elastance ($E_{es,lv}$) from 2.5 mmHg/mL to 0.75 mmHg/mL and parameter A from 1 mmHg to 0.65 mmHg in the left ventricle model, and increasing the left ventricular zero-pressure volume ($V_{lv,0}$) from 15 mL to 25 mL. A downward shift occurs in the cerebral flow rate autoregulatory curve [6] which results in decreased cerebral blood flow rate in patients with heart failure [37]. Downward shift in the cerebral flow rate autoregulatory curve was simulated reducing the aortic pressure set point in the cerebral flow autoregulatory function ($p_{ao,cbf,set}$) from 93 mmHg to 75 mmHg in the numerical model simulating heart failure with reduced ejection fraction.

2.3.3. Impaired cerebral flow rate autoregulatory function

Cerebral autoregulatory function may be impaired or may remain absent in certain conditions such as ischaemic stroke, traumatic brain injury, infections like meningitis or malignant hypertension [38–41]. Impaired cerebral autoregulatory function was simulated by keeping the resistance of pial circulation (R_{pc}) constant at 3.6 mmHg s/mL. High arterial blood pressure as in malignant hypertension with impaired cerebral autoregulation as described in [41] was simulated by increasing the peripheral arterial resistance from 0.75 mmHg s/mL to 2 mmHg s/mL.

2.3.4. Hypercapnia and hypocapnia

Hypercapnia is caused by arterial CO_2 partial pressure higher than 42 mmHg [42] and hypocapnia is caused a decrease in CO_2 partial pressure in the arteries below 35 mmHg [43]. Both conditions alter cerebral blood flow rate and effect of hypercapnia is increasing the cerebral flow rate whereas hypocapnia reduces it [44]. Hypercapnia was simulated by increasing the arterial CO_2 partial pressure to 50 mmHg from 40 mmHg and hypocapnia was simulated by decreasing the arterial CO_2 partial pressure to 30 mmHg from 40 mmHg.

2.3.5. Hypoxemia

Hypoxemia is caused by a decrease in the partial pressure of oxygen in the blood [45]. The cerebral vasculature responds partial pressure of arterial oxygen around 50 ~ 53 mmHg [46,47]. Hypoxemia was simulated by reducing oxygen partial pressure in the arteries to 45 mmHg from 100 mmHg.

2.3.6. Simulation of cerebral blood flow rate regulation curves

Static cerebral autoregulation curve is evaluated by infusing phenylephrine continuously to increase systemic arteriolar resistance and arterial blood pressure without altering myocardial contractility [48]. Therefore, static cerebral autoregulatory functions in the numerical models simulating normophysiology, heart failure with reduced ejection fraction and impaired cerebral autoregulatory function were evaluated by increasing the systemic arteriolar resistance (R_{ars}) iteratively in each simulation between 60 mmHg and 150 mmHg mean aortic pressure. CO_2 and O_2 cerebral vascular reactivities were evaluated by increasing the partial pressures of CO_2 and O_2 in arteries from 20 mmHg to 100 mmHg and 30 mmHg and 180 mmHg respectively.

2.4. Sensitivity analysis

Parameters modified manually to simulate different physiological scenarios were systolic elastance ($E_{es,lv}$), parameter A and zero-pressure volume ($V_{0,lv}$) in the compartment simulating left ventricular function, systemic arteriolar resistance (R_{ars}) in the blood circulatory system, arterial CO_2 and O_2 pressures (p_{CO2}, p_{O2}) and aortic pressure set point in the cerebral flow autoregulatory function ($p_{ao,cbf,set}$). Therefore, sensitivity of the mean cerebral flow rate on these parameters was evaluated using Matlab Simulink Sensitivity Analyzer application. Values of the parameters used in the cardiovascular numerical model changes within a large range for different physiological cases and healthy conditions. Fifty samples for each parameter were generated randomly using uniform distributions. Uniform distribution was used in the sensitivity analysis to assign equal probability to all values between its minimum and maximum. Upper and lower values of the variables in the sensitivity analysis were selected considering the physiological range of the elastance ($E_{es,lv}$), parameter A and zero-pressure volume ($V_{0,lv}$) in the compartment simulating left ventricular function, systemic arteriolar resistance (R_{ars}) [31] whereas upper and lower values of arterial CO_2 and O_2 pressures (p_{CO2}, p_{O2}) were selected according data used in the curve fitting (Tables 2 and 3). Upper and Lower values of the aortic pressure set point in the cerebral flow autoregulatory function ($p_{ao,cbf,set}$) were determined considering the pressures in healthy and heart failure conditions in previously published studies [21]. Upper and lower values

for the samples for each parameter are given in Table 4. Scatter plots and histograms for the samples used in the sensitivity analysis is given in Fig. 2.

Overlay linear fit lines utilising R-values were used to evaluate correlation between the total cerebral blood flow rate and the variables evaluated in the sensitivity analysis. Tornado plot was used to compare the relative importance of variables.

3. Results

Initially, coefficients in the cerebrovascular CO_2 and O_2 reactivities were determined using Curve Fitting Toolbox in Matlab R2021b to describe cerebral autoregulatory mechanisms and interaction among them. Coefficients in the equations describing the cerebrovascular CO_2 and O_2 reactivities (Eq. (1) and Eq. (2)) are given in Table 5 and the curves fit to simulate cerebrovascular CO_2 and O_2 reactivities are given in Fig. 3. Coefficient of determination (R^2) values in curve fitting for both models were around 0.99. Cerebral autoregulation curves simulating cerebrovascular CO_2 and O_2 reactivities, static cerebral autoregulation curve in normophysiology and heart failure with reduced ejection fraction, impaired cerebral autoregulation curve are given in Fig. 4.

Cerebral flow rate increased rapidly with increase of arterial CO_2 pressure whereas there was a rapid decrease in cerebral flow rate until arterial O_2 pressure reduced around 60 mmHg. It remained constant between 60 mmHg and 180 mmHg arterial O_2 pressures. Cerebral blood flow rate remained constant between 60 mmHg and 150 mmHg mean arterial blood pressures in the numerical model simulating normal cardiovascular physiology and cerebral autoregulatory mechanisms. Static autoregulatory curve plateau shifted down in the numerical model simulating heart failure with reduced ejection fraction where cerebral flow rate increased with increasing mean arterial blood pressures between 60 mmHg and 135 mmHg. Ther was no plateau in the cerebral autoregulatory curve and cerebral blood flow rate increased with increasing mean arterial blood pressure in the numerical model simulating impaired cerebral autoregulation. Cerebral blood flow rate, cardiac output, mean aortic pressure, ejection fraction, pial circulation and systemic arteriolar resistances in the numerical models simulating normophsyiology, heart failure with reduced ejection fraction, impaired cerebral autoregulation during malignant hypertension, hypercapnia, hypocapnia and hypoxemia are given in Table 6. Left ventricular and aortic pressures, right ventricular and pulmonary arterial pressures, left and right ventricular volumes and blood flow rates in the right internal carotid, vertebral and middle cerebral arteries in the numerical model simulating normal cardiovascular physiology and cerebral autoregulatory mechanisms are given in Fig. 5.

Left ventricular and aortic systolic pressures were around 120 mmHg whereas right ventricular and pulmonary arterial systolic pressure were around 35 mmHg. Right ventricular volume remained higher than left ventricular volume over a cardiac cycle. Flow rates in the internal carotid, vertebral and middle cerebral arteries over a cardiac cycle changed between 155 mL/min and 500 mL/min, 47 mL/min and 150 mL/min and 80 mL/min and 250 mL/min respectively. Left ventricular and aortic pressures, right ventricular and pulmonary arterial pressures, left and right ventricular volumes and blood flow rates in the right internal carotid, vertebral and middle cerebral arteries in the numerical model simulating heart failure with ejection fraction are given in Fig. 6.

Left ventricular and aortic systolic pressures reduced to 91 mmHg whereas right ventricular and pulmonary arterial systolic pressure were around 37 mmHg. Left and right ventricular volumes over a cardiac cycle changed between 128 mL and 175 mL and 74 mL and 121 mL, respectively. Flow rates in the internal carotid, vertebral and middle cerebral arteries over a cardiac cycle changed between 150 mL/min and 375 mL/min, 45 mL/min and 113 mL/min and 77 mL/min and 190 mL/min respectively. Left ventricular and aortic pressures, right ventricular and pulmonary arterial pressures, left and right ventricular volumes and blood flow rates in the right internal carotid, vertebral and middle cerebral arteries in the numerical model simulating impaired cerebral autoregulation due to malignant hypertension are given in Fig. 7.

Left ventricular and aortic systolic pressures were 183 mmHg whereas right ventricular and pulmonary arterial systolic pressure were around 33 mmHg. Left and right ventricular volumes over a cardiac cycle changed between 51 mL and 116 mL and 69 mL and 134 mL, respectively. Flow rates in the internal carotid, vertebral and middle cerebral arteries over a cardiac cycle changed between 381 mL/min and 751 mL/min, 115 mL/min and 226 mL/min and 195 mL/min and 377 mL/min respectively. Blood flow rates in the right internal carotid, vertebral and middle cerebral arteries in the numerical model simulating hyper and hypocapnia are given in Fig. 8.

Internal carotid, vertebral and middle cerebral arterial flow rates over a cardiac cycle changed between 242 mL/min and 587 mL/min, 73 mL/min and 177 mL/min and 124 mL/min and 295 mL/min in the numerical model simulating hypercapnia. Internal carotid, vertebral and middle cerebral arterial flow rates over a cardiac cycle changed between 72 mL/min and 416 mL/min, 22 mL/min and 125 mL/min and 38 mL/min and 208 mL/min in the numerical model simulating hypocapnia. Blood flow rates in the right internal carotid, vertebral and middle cerebral arteries in the numerical model simulating hypoxemia are given in Fig. 9.

Internal carotid, vertebral and middle cerebral arterial flow rates over a cardiac cycle changed between 250 mL/min and 595 mL/min, 76 mL/min and 180 mL/min and 129 mL/min and 300 mL/min in the numerical model simulating hypoxemia. Overlay linear fit in the sample scatter plots for each parameter evaluated in the sensitivity analysis and histogram for the mean cerebral blood flow rate is given in Fig. 10.

Overlay linear fit line in the scatter plots show that the arterial CO_2 pressure ($p_{a,CO2}$) is positively related with the cerebral blood flow rate and there is high correlation between these two parameters whereas arterial O_2 pressure ($p_{a,O2}$) is negatively corelated with the cerebral blood flow rate. Left ventricular systolic elastance ($E_{es,lv}$) which describes the active contraction properties of the left ventricle is negatively correlated with cerebral blood flow rate whereas A_{lv} which describes the passive contraction properties of the left ventricle is positively correlated with cerebral blood flow rate. Left ventricular zero-pressure volume ($V_{0,lv}$), systemic arteriolar resistance (R_{ars}) and aortic pressure set point in the cerebral flow autoregulatory function ($p_{ao,cbf,set}$) are positively correlated with the cerebral blood flowrate. The tornado plot showing the correlation of the parameters with the mean cerebral flow rate in the numerical model is given in Fig. 11.

There was a high correlation between arterial CO_2 pressure ($p_{a,CO2}$) and cerebral blood flow rate. Aortic pressure set point in the cerebral flow autoregulatory function ($p_{ao,cbf,set}$) and arterial O_2 pressure influenced cerebral blood flow rate relatively less with respect to arterial CO_2 pressure ($p_{a,CO2}$) in the numerical model. Left ventricular systolic elastance had the least influence on cerebral blood flow rate when compared with the influence of the other parameter evaluated in the

Table 4
Sample upper and lower values for the parameters evaluated in the sensitivity analysis. $E_{es,lv}$, A, $V_{0,lv}$, R_{ars}, $p_{a,CO2}$, $p_{a,O2}$ and $p_{ao,cbf,set}$ represent left ventricular systolic elastance, parameter A in the left ventricle model, left ventricular zero-pressure volume, systemic arteriolar resistance, arterial pressures of CO_2 and O_2 and aortic pressure set point in the cerebral flow autoregulatory function, respectively.

	Lower Value	Upper Value
$E_{max,lv}$ [mmHg/mL]	0.5	3
A [mmHg]	0.6	1.2
$V_{0,lv}$ [mL]	10	30
R_{ars} [mmHg s/mL]	0.2	2.5
$p_{a,CO2}$ [mmHg]	20	100
$p_{a,O2}$ [mmHg]	35	180
$p_{ao,cbf,set}$ [mmHg]	70	100

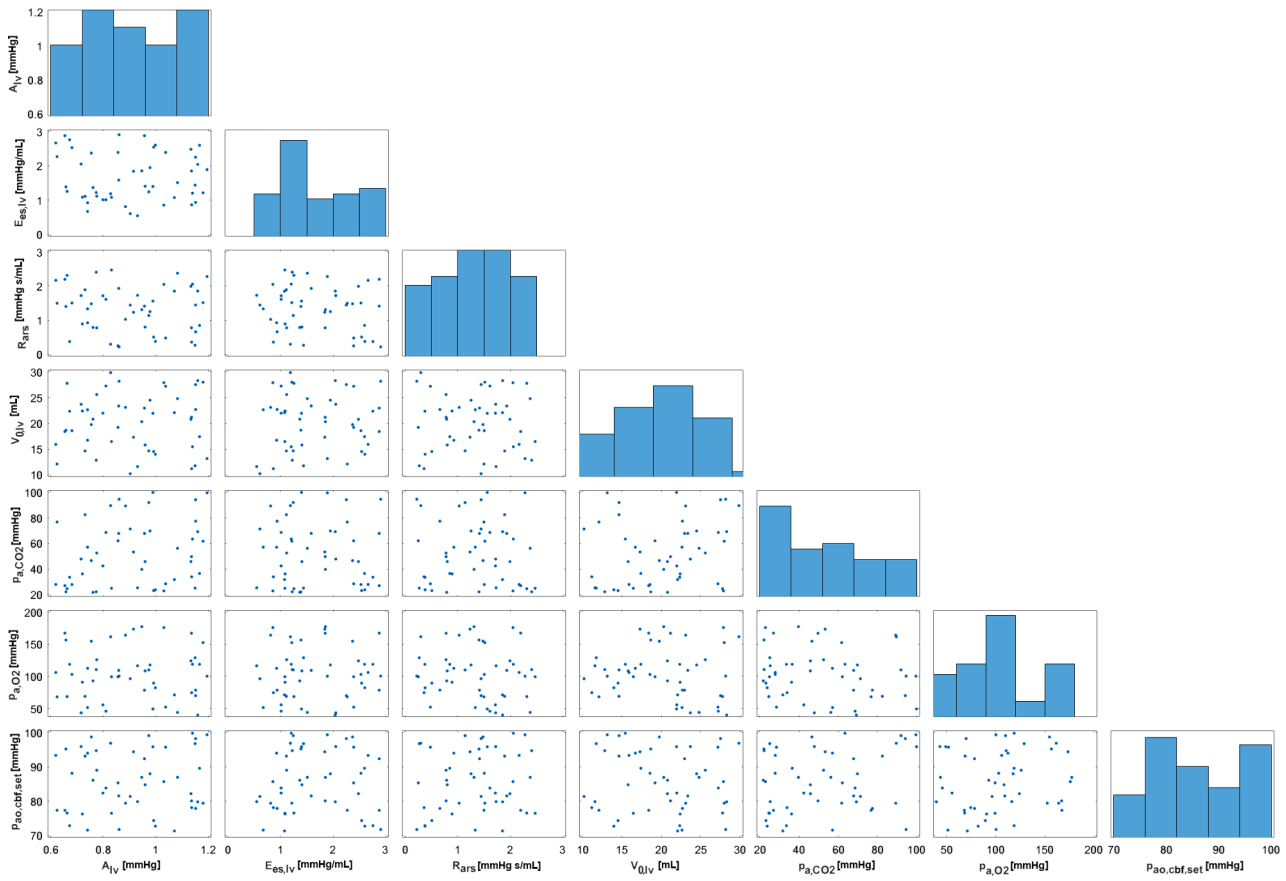

Fig. 2. Scatter plots and histograms for the sample distributions in the sensitivity analysis. $E_{es,lv}$, A_{lv}, $V_{0,lv}$, R_{ars}, $p_{a,CO2}$, $p_{a,O2}$ and $p_{ao,cbf,set}$ represent left ventricular systolic elastance, parameter A in the left ventricle model, left ventricular zero-pressure volume, systemic arteriolar resistance, arterial pressures of CO_2 and O_2 and aortic pressure set point in the cerebral flow autoregulatory function, respectively.

Table 5
Coefficients in the equations describing the cerebral flow rate CO_2 and O_2 reactivities (a and b are the coefficients and the numbers show the coefficient indices in Eq.1 and Eq.2).

		1	2	3	4
CO_2 reactivity	a	9.025	−0.055	–	–
O_2 reactivity	b	1.042	−0.00026	−10.96	−0.0694

sensitivity analysis.

4. Discussion

In this study, interaction among static cerebral autoregulation, cerebrovascular CO_2 and O_2 reactivities and systemic arterial resistance regulation was simulated to evaluate cerebral blood flow rate in different physiological scenarios. Also, new models have been developed to simulate cerebrovascular CO_2 and O_2 reactivities. A one-term exponential model was used to simulate cerebrovascular CO_2 reactivity whereas cerebrovascular O_2 reactivity was simulated using a two-

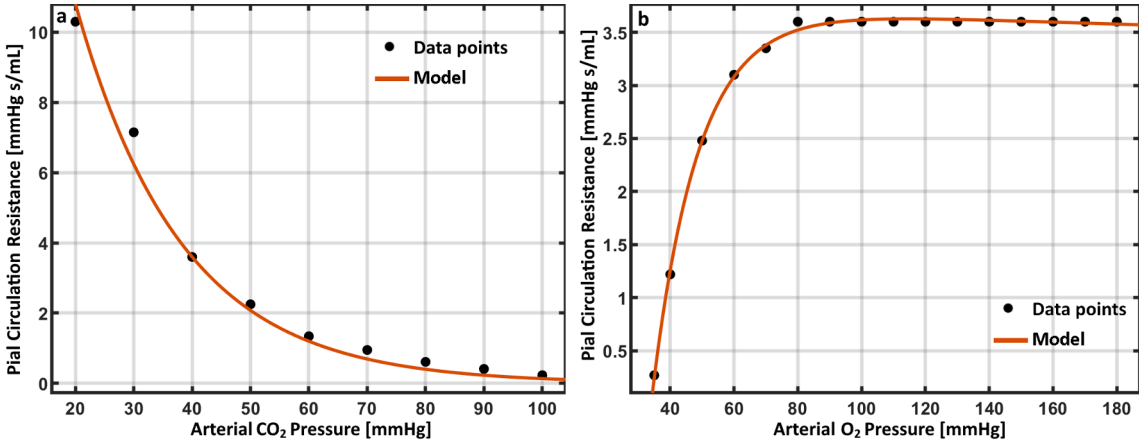

Fig. 3. Curve fit to simulate cerebral flow rate (a) CO_2 reactivity and (b) O_2 reactivity.

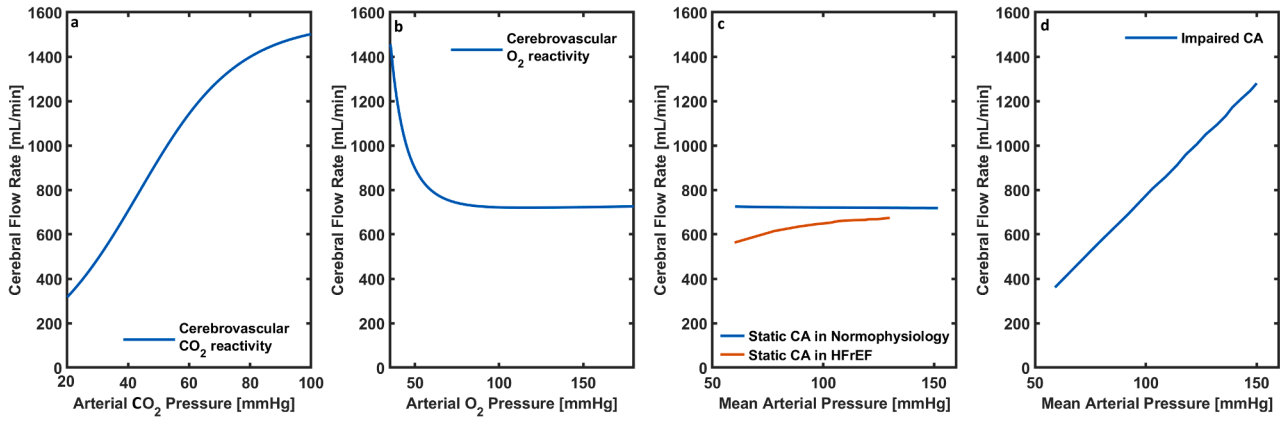

Fig. 4. Cerebral autoregulation (CA) curves for (a) cerebrovascular CO_2 reactivity, (b) cerebrovascular O_2 reactivity, (c) Static CA in the numerical models simulating normophysiology and heart failure with reduced ejection fraction (HFrEF), (d) impaired CA.

Table 6
Cerebral blood flow rate (CBF), cardiac output (CO), mean aortic pressure (MAP), systolic and diastolic aortic pressures ($p_{ao,sys}$, $p_{ao,dias}$) ejection fraction (EF), pial circulation and systemic arteriolar resistances (R_{pc}, R_{ars}) in the numerical models simulating normophsyiology, heart failure with reduced ejection fraction (HFrEF), impaired cerebral autoregulation (CA) during malignant hypertension, hypercapnia, hypocapnia and hypoxemia. (* shows the R_{ars} value adjusted manually to simulate malignant hypertension in the numerical model with impaired CA).

	CBF [mL/min]	CO [L/min]	MAP [mmHg]	$p_{ao,sys}$ [mmHg]	$p_{ao,dias}$ [mmHg]	EF [%]	R_{pc} [mmHgs/mL]	R_{ars} [mmHgs/mL]
Normophysiology	721	5.06	93	119	78	54.78	3.62	0.75
HFrEF	606	3.47	74	90	64	26.50	3.50	1
Impaired CA	1313	4.89	153	182	138	56.28	3.62	2*
Hypercapnia	950	5.09	91	117	76	55.25	2	0.77
Hypocapnia	504	5.02	95	120	80	54.38	6.52	0.73
Hypoxemia	972	5.09	91	117	76	55.29	1.89	0.77

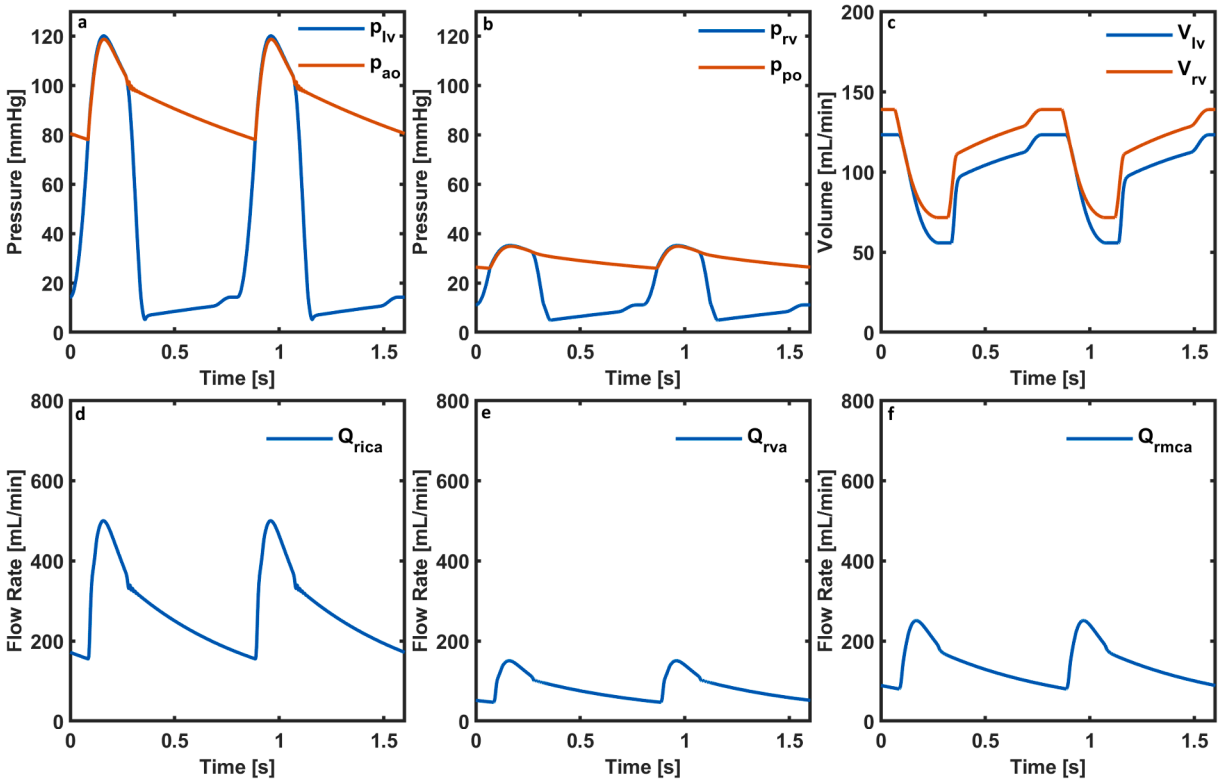

Fig. 5. (a) Left ventricular and aortic pressures (p_{lv}, p_{ao}), (b) right ventricular and pulmonary arterial pressures (p_{rv}, p_{po}), (c) left and right ventricular volumes (V_{lv}, V_{rv}) and blood flow rates in the (d) right internal carotid (Q_{rica}), (e) right vertebral (Q_{rva}) and (f) right middle cerebral arteries (Q_{rmca}) in the numerical model simulating normal cardiovascular physiology and cerebral autoregulatory mechanisms.

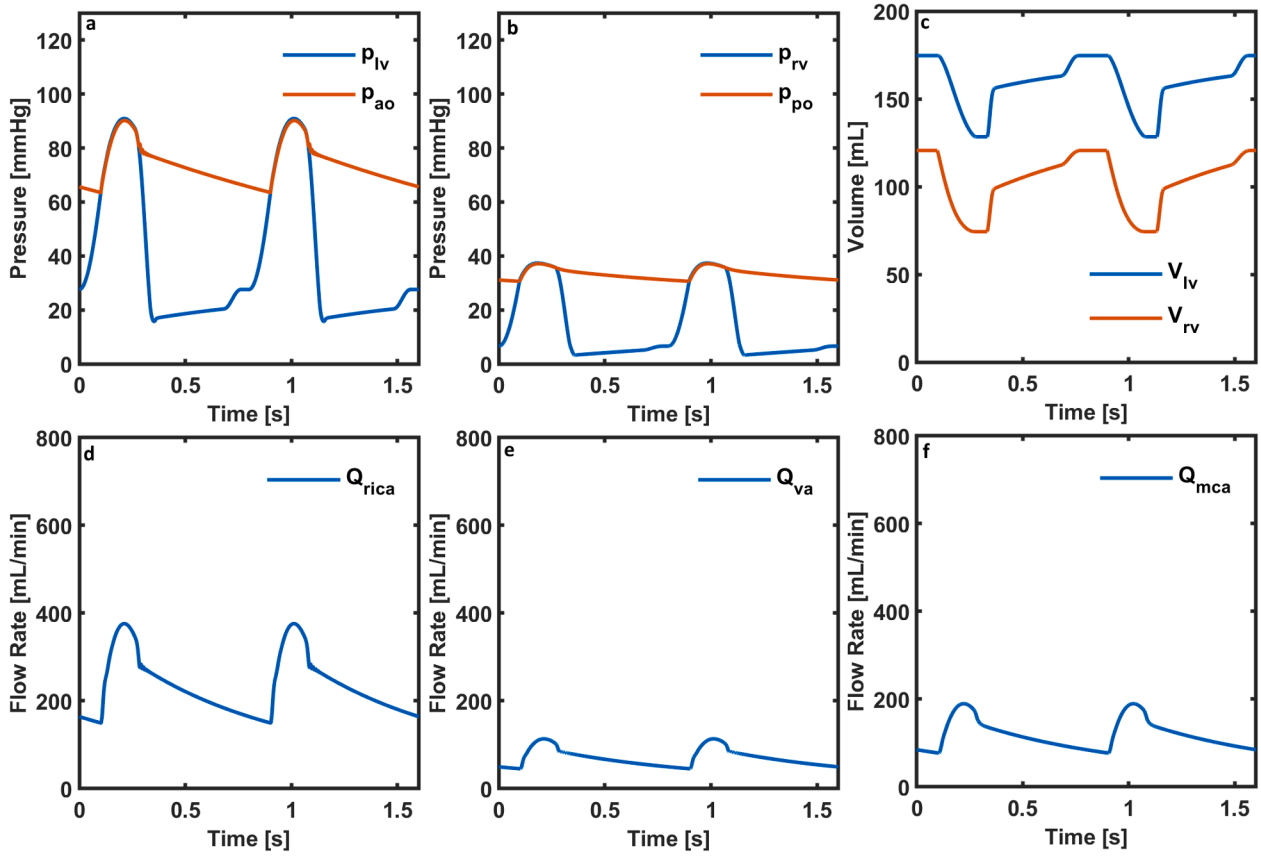

Fig. 6. (a) Left ventricular and aortic pressures (p_{lv}, p_{ao}), (b) right ventricular and pulmonary arterial pressures (p_{rv}, p_{po}), (c) left and right ventricular volumes (V_{lv}, V_{rv}) and blood flow rates in the (d) right internal carotid (Q_{rica}), (e) right vertebral (Q_{rva}) and (f) right middle cerebral arteries (Q_{mca}) in the numerical model simulating heart failure with reduced ejection fraction.

term exponential model. The plateau in the cerebrovascular O_2 reactivity after 80 mmHg arterial O_2 pressure (Fig. 3b) was simulated by the two-term exponential with high accuracy. Coefficient of determination (R^2) values in the curve fitting was around 0.99 for both CO_2 and O_2 cerebrovascular reactivities suggesting that the developed models can simulate the cerebral blood flow rate with respect to varying values of arterial CO_2 and O_2 pressures with a good accuracy. Lower and upper limits of the arterial CO_2 and O_2 pressure data used to develop cerebrovascular CO_2 and O_2 reactivities were 20 mmHg and 100 mmHg and 35 mmHg and 180mmg, respectively. Therefore, CO_2 and O_2 cerebrovascular reactivity models work accurately within these limits. Structure of the developed concept models simulating cerebrovascular CO_2 and O_2 reactivities will be the same for the given data intervals. Coefficients in the developed models may be different if additional data is used, however, such a difference is also expected if personalised simulations are performed using patient specific data.

Curve fitting for the cerebrovascular CO_2 and O_2 reactivities was done considering the isolated effects of each mechanism on the resistance of the pial circulation (R_{pc}). Therefore, resistance of the pial circulation (R_{pc}) was normalised using the set value ($R_{pc,set}$, Eqs. 6–8) and interaction of the cerebral autoregulatory mechanisms was modelled using the normalised values (Eq. (5)). Also, scaling coefficients in the exponential models used to simulate cerebrovascular CO_2 and O_2 reactivities included the set value for resistance of the pial circulation ($R_{pc,set}$). This assumption allows the set value ($R_{pc,set}$) to play role on the response of the cerebrovascular CO_2 and O_2 reactivities. Impaired static autoregulatory function in the numerical model simulating heart failure was described by reducing the set value for the aortic pressure ($p_{ao,cbf,set}$) from 93 mmHg to 75 mmHg to simulate the total cerebral flow rate as reported in [37]. Parameters in the compartment describing the left ventricular function was modified considering a systolic heart failure as described in [31].

Detailed description of the cerebral circulation in this study allows simulating blood flow rates in different compartments such middle cerebral arteries where the cerebral blood flow is usually evaluated from. Relatively simple models describing cerebral circulation with less compartments as described in [10,49] simulate only total cerebral blood flow rate. In this study, cerebral circulation is included Circle of Willis and pial circulation. Therefore, the simulation results can be compared to clinical data. Also, cerebral autoregulation in pial arteries is integrated into the model to simulate changes in the cerebral blood flow rate for different physiological cases in a realistic way. Previously developed models describing cerebrovascular autoregulation simulate cerebral circulation with less compartments or present isolated effects of certain autoregulation mechanisms [8–11,15,17]. Presented cerebral flow rate autoregulation model in this study simulates combined effects of systemic arteriolar baroreflex control, static cerebral autoregulatory function and cerebrovascular CO_2 and O_2 reactivities using a detailed cerebral circulation model. More detailed studies simulating cerebral autoregulation and cerebrovascular CO_2 reactivity with a detailed as presented in [13,18] does not include cerebrovascular O_2 reactivity as presented in the current study. Also, altered static cerebral autoregulation during heart failure was simulated using aortic pressure set point in the cerebral flow autoregulatory function in this study.

In healthy adults average total cerebral blood flow rate is around 717 mL/min [32] within a large variation range [50]. Numerical model simulated 721 mL/min mean cerebral flow rate (Table 6) for the simulated healthy condition. Weakened ventricular contractions in heart failure results in reduced cardiac output and arterial blood flow rate. Decreased stretching of pressure baroreceptors enhance sympathetic

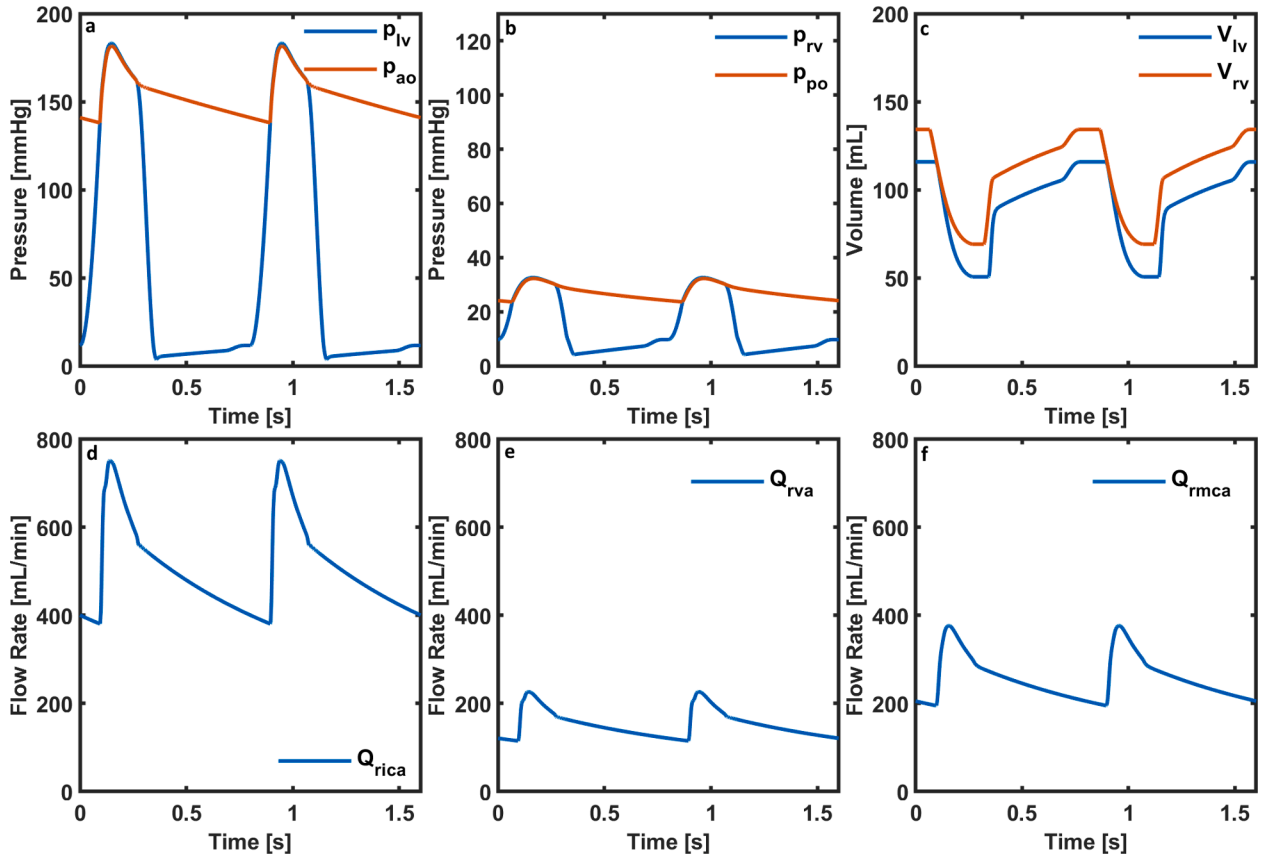

Fig. 7. (a) Left ventricular and aortic pressures (p_{lv}, p_{ao}), (b) right ventricular and pulmonary arterial pressures (p_{rv}, p_{po}), (c) left and right ventricular volumes (V_{lv}, V_{rv}) and blood flow rates in the (d) right internal carotid (Q_{rica}), (e) right vertebral (Q_{rva}) and (f) right middle cerebral arteries (Q_{mca}) in the numerical model simulating impaired cerebral autoregulation due to malignant hypertension.

tone resulting in increased peripheral vascular resistance [51]. Numerical model simulated this mechanism by increasing the systemic arteriolar resistance to 1 mmHg s/mL from 0.75 mmHg s/mL (Table 6). Moreover, sensitivity analysis showed that there is a positive correlation between the systemic arteriolar resistance and cerebral blood flow rate. However, static cerebral autoregulatory curve is shifted down in patients with heart failure [6] reducing the cerebral blood flow rate in these patients [37]. This mechanism was simulated by using different aortic pressure set points for static cerebral autoregulation and systemic arteriolar resistance regulation ($p_{ao,cbf,set}$, $p_{ao,ars,set}$). A downward shift in the static cerebral autoregulatory curve (Fig. 4c) and decrease in the cerebral blood flow rate in the simulations (Table 6) were achieved by reducing the aortic pressure set points for static cerebral autoregulation ($p_{ao,cbf,set}$) to 75 mmHg from 93 mmHg whilst systemic arteriolar resistance increased.

Static cerebral autoregulation function may be impaired due to malignant hypertension [41] as simulated by the numerical model. Malignant hypertension is caused by renovascular diseases, endocrine dysfunction, coarctation of aorta or central nervous system disorders [52]. In this study, increased systemic vascular resistance simulated similar conditions to coarctation of aorta. Pial circulation resistance (R_{pc}) was kept at 3.6 mmHgs/mL to simulate impaired cerebral autoregulation. Keeping pial circulation resistance (R_{pc}) at constant value simulated only passive dilation of the blood vessels in pial circulation compartment due to increased blood pressure and flow rate. Moreover, a linear relation as reported in [41] was simulated between mean aortic pressure and cerebral blood flow (Fig. 4d).

Arterial CO_2 pressure ($p_{a,CO2}$) around 50 mmHg in hypercapnic subjects may increase the cerebral flow rate between 40 percent and 180 percent [53]. In this study, 50 mmHg arterial CO_2 pressure ($p_{a,CO2}$) increased cerebral blood flow rate from 721 mL/min to 950 mL/min (Table 6) resulting in 33 percent change in cerebral blood flow rate. On the other hand, 30 mmHg arterial CO_2 pressure ($p_{a,CO2}$) in haypocapnic subjects as simulated in this study may result in 30 percent to 50 percent decrease in cerebral blood flow rate [53]. In this study, cerebral blood flow rate reduced from 721 mL/min to 504 mL/min at 30 mmHg arterial CO_2 pressure ($p_{a,CO2}$) resulting in 30 percent change in cerebral blood flow rate. Therefore, the simulation results for hyper and hypocapnia are in a good agreement with the data reported in the literature.

Cerebral blood flow rate increases with the arterial O_2 pressure ($p_{a,O2}$) lower than 50 mmHg [28]. Moreover, different mechanisms such as chemical and metabolic mechanisms, neurogenic mechanism or nitric oxide may also influence hypoxemic response of cerebral blood flow rate [28]. Although hypoxemia profoundly increases cerebral blood rate, the increase may vary in different subjects. In this study, hypoxemia simulated by adjusting the arterial O_2 pressure ($p_{a,O2}$) to 50 mmHg increased cerebral blood flow rate from 721 mL/min to 972 mL/min. This corresponds to 35 percent increase in cerebral blood flow rate and in a good with the data reported in [28].

Blood flow rate signals in the right internal carotid artery, right vertebral artery and right middle cerebral artery are presented for each case in this study. The reason for choosing these compartments was blood is carried to the cerebral circulation by the internal carotid and vertebral arteries in the numerical model. Also, cerebral blood flow is usually evaluated from the middle cerebral arteries because the thinnest site in adult skull is where the middle cerebral arteries are located [54]. The flow rate in the internal carotid arteries changed between 155 mL/min and 500 mL/min over a cardiac cycle. Additionally, the flow rate in the vertebral arteries changed between 47 mL/min and 150 mL/min over a cardiac cycle. The variation range of the flow rate in the internal

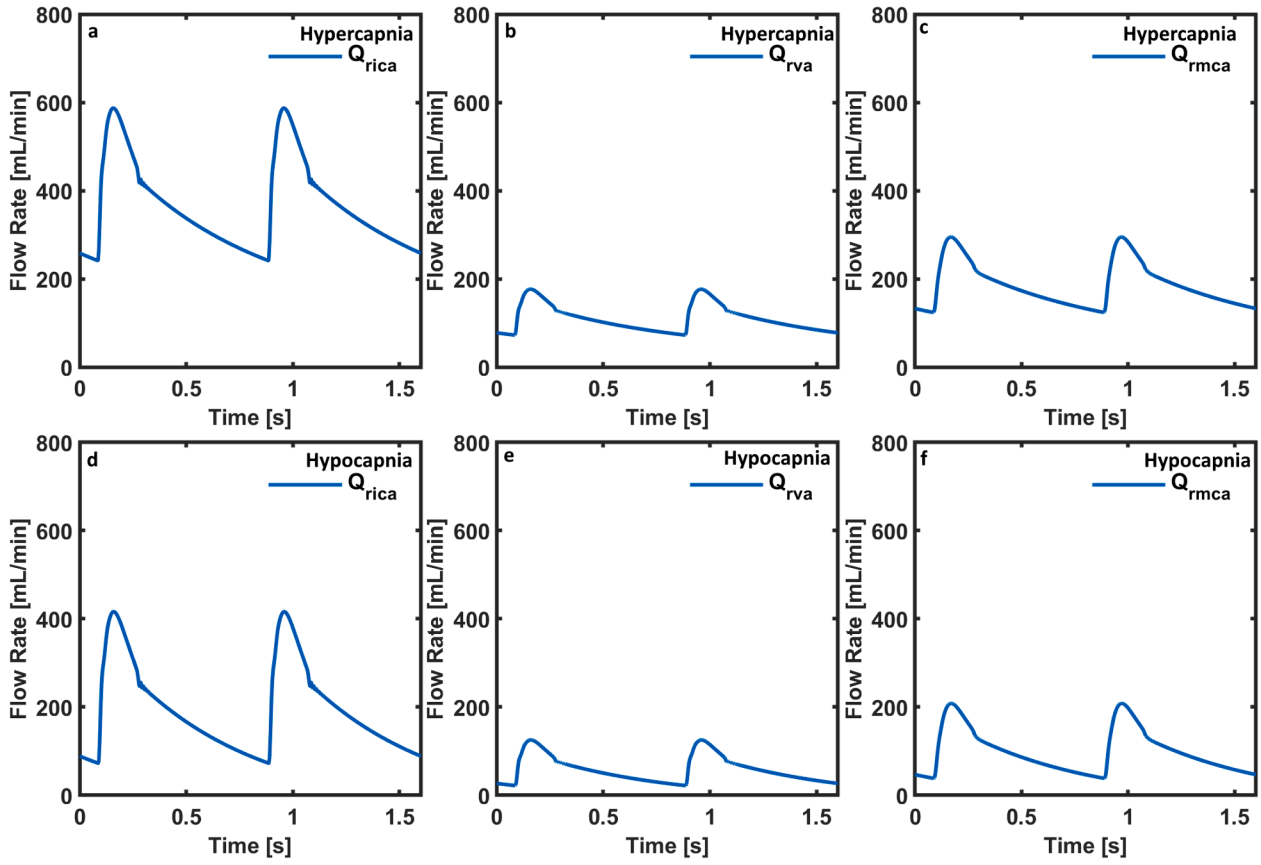

Fig. 8. Blood flow rates in the (a) right internal carotid artery (Q_{rica}), (b) vertebral artery (Q_{rva}) and (c) middle cerebral artery (Q_{mca}) during hypercapnia, blood flow rate in the (d) right internal carotid artery (Q_{rica}), (e) right vertebral artery (Q_{rva}) and (f) right middle cerebral artery (Q_{mca}) during hypocapnia.

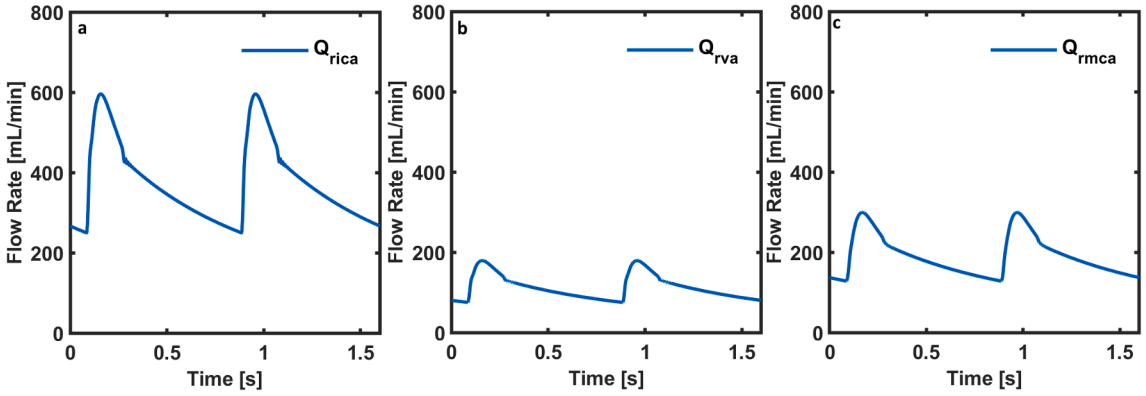

Fig. 9. Blood flow rates in the (a) right internal carotid artery (Q_{rica}), (b) right vertebral artery (Q_{rva}) and (c) right middle cerebral artery (Q_{mca}) during hypoxemia.

carotid arteries and vertebral arteries is quite high and the average of flow rate signals obtained from the clinical data [55] shows a similar variation range with the flow rate signals simulated in the healthy cardiovascular system over a cardiac cycle. Also pressures in the ventricles, aorta and pulmonary arteries and ventricular volumes remained within a physiological range for the healthy condition [29] in the numerical model simulating normophysiology (Fig. 5). Systolic left ventricular failure results in reduced systolic pressures in the left ventricle and aorta whereas right ventricular and pulmonary arterial pressures at the systole increase [56]. There is also an increase in the overall left ventricular volume whilst ventricular stroke volumes and ejection fraction reduce [56]. Ventricular, aortic and pulmonary arterial pressures and ventricular volumes followed similar trends in the numerical model simulating heart failure with reduced ejection fraction (Fig. 6). Reduced middle cerebral arterial blood flow rate in the simulations also confirms the validity of the results for heart failure with reduced ejection fraction [57]. Malignant hypertension increased the systolic left ventricular pressure and aortic pressure which resulted in increased internal carotid, vertebral and middle cerebral arterial flow rates although the cardiac output slightly decreased with respect to healthy condition (Fig. 7). Impaired cerebral autoregulation results in similar physiological outcome in malignant hypertension [41]. Blood flow rates in the internal carotid and middle cerebral arteries increase in hypercapnia and decrease in hypocapnia [58]. Similar results were simulated in the numerical models simulating hypercapnia and hypocapnia (Fig. 8). Also hypoxemia increases the cerebral blood flow rates [45]. Increased flow rates in the internal carotid, vertebral and middle cerebral arteries in the numerical model simulating hypoxemia (Fig. 9) is coherent with clinical

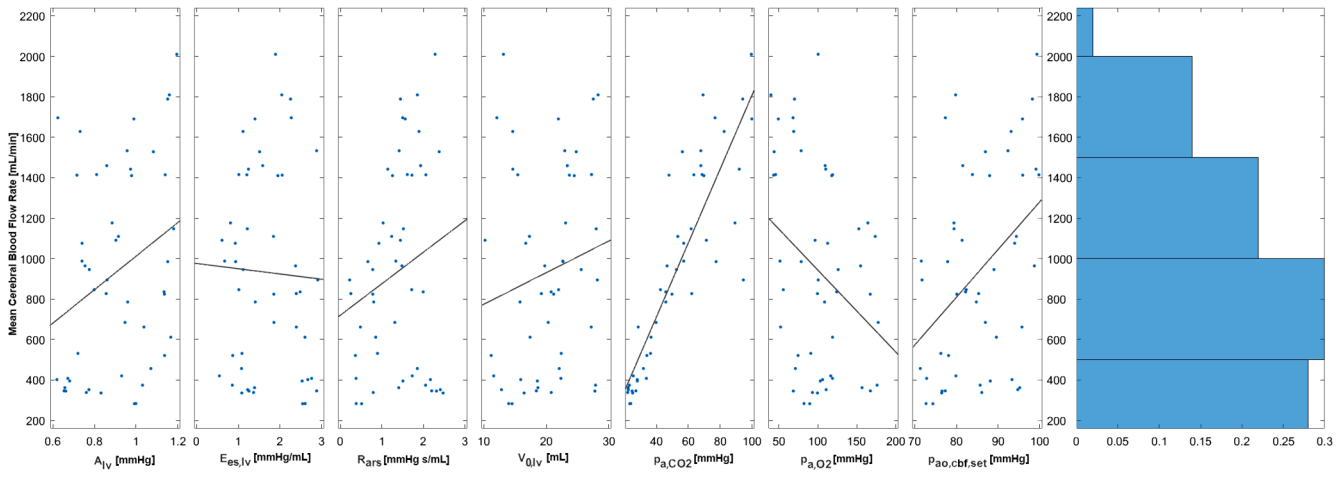

Fig. 10. Overlay linear fit in the sample scatter plots for each parameter evaluated in the sensitivity analysis and histogram for the mean cerebral blood flow rate. $E_{es,lv}$, A_{lv}, $V_{0,lv}$, R_{ars}, $p_{a,CO2}$, $p_{a,O2}$ and $p_{ao,cbf,set}$ represent left ventricular systolic elastance, parameter A in the left ventricle model, left ventricular zero-pressure volume, systemic arteriolar resistance, arterial pressures of CO_2 and O_2 and aortic pressure set point in the cerebral flow autoregulatory function, respectively.

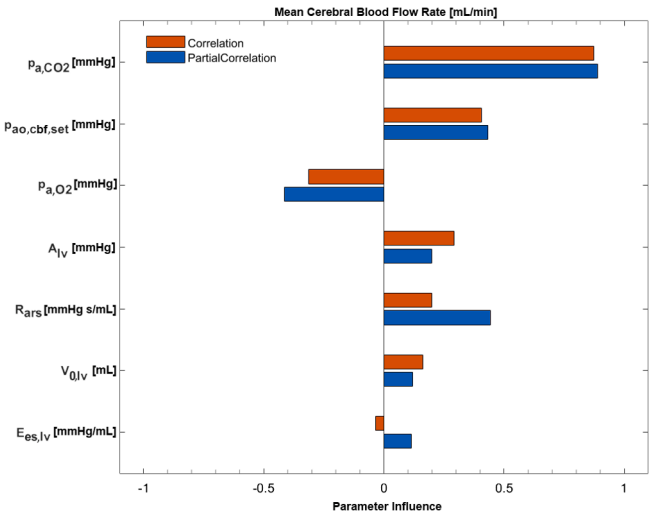

Fig. 11. Correlation of the parameters with the mean cerebral flow rate in the numerical model. $E_{es,lv}$, A_{lv}, $V_{0,lv}$, R_{ars}, $p_{a,CO2}$, $p_{a,O2}$ and $p_{ao,cbf,set}$ represent left ventricular systolic elastance, parameter A in the left ventricle model, left ventricular zero-pressure volume, systemic arteriolar resistance, arterial pressures of CO_2 and O_2 and aortic pressure set point in the cerebral flow autoregulatory function, respectively.

findings. Although overall flow rates were different in the simulated physiological cases, amplitude of the flow rate signals remained similar for each cerebral circulation compartment in the numerical models simulating normophysiology, hypercapnia, hypocapnia and hypoxemia. This was because systolic and diastolic aortic pressures and amplitude of the aortic pressure signal in these physiological cases were also similar (Table 6). Ito et al [59] reported similar systolic and diastolic aortic pressures in normocapnic, hypercapnic and hypocapnic subjects undergone ^{11}CO positron emission tomography measurements confirming the validity of the simulations. Decreased aortic pressure signal amplitude in the numerical model simulating heart failure with reduced ejection also reduced blood flow rate amplitudes in the right internal carotid artery, right vertebral artery and right middle cerebral artery whereas increased aortic pressure signal amplitude in the numerical model simulating impaired static cerebral autoregulation increased blood flow rate amplitudes in these compartments.

Sensitivity analysis showed that cerebral blood flow rate is positively correlated with arterial CO_2 pressure ($p_{a,CO2}$) and highly sensitive to changes to changes in this parameter (Fig. 11). Such a relation between cerebral blood flow rate and arterial CO_2 pressure ($p_{a,CO2}$) has already been reported in the literature [60]. Altered aortic pressure set point in the cerebral flow autoregulatory function ($p_{ao,cbf,set}$) were also had a profound influence on the cerebral blood flow rate which may explain downward shift in the static cerebral autoregulation curve in patients affected by heart failure. Sensitivity analysis showed that left ventricular systolic elastance which describes the cardiac contractility had the least effect on cerebral blood flow rate (Fig. 11) among the evaluated parameters. Moreover, it was negatively correlated with the cerebral blood flow rate. It has already been reported that increased cardiac contractility has a little effect on the carotid arterial blood flow rate with a negative correlation [61] confirming the validity of the simulations. On the other hand parameter A ($A_{lv,}$ Eq. (11)) which describes the passive contraction properties of the had a more profound effect on the cerebral flow rate (Fig. 11). Such a result show that left ventricular filling properties has more influence on the cerebral blood flow rate when compared with left ventricular contraction properties in the numerical model.

Numerical model presented in this study has limitations. Recent studies show that static cerebral autoregulation function regulates the cerebral blood flow rate for slow changes in arterial blood pressure [62]. Dynamic changes in arterial blood pressure during daily activities such as sit to stand or acute exercise affect cerebral blood flow rate causing fluctuations in blood flow rate in cerebral circulation [62]. In this study, dynamic regulation of cerebral blood flow rate has not been modelled because, a case study such as acute exercise has not been considered. Static cerebral autoregulatory curve regulates cerebral blood flow rate only over the plateau between 60 mmHg and 150 mmHg. Hypo and hyper cerebral perfusion and reserve capacity of the cerebral vessel has not been included in the static cerebral autoregulation curve. Nonetheless, simulated physiological cases remain within capability of the numerical model and has a good agreement with data reported in the literature. CO_2 and O_2 cerebrovascular reactivities are described within 20 mmHg an 100 mmHg arterial CO_2 pressure ($p_{a,CO2}$) and 35 mmHg an 180 mmHg arterial O_2 pressure ($p_{a,O2}$). However, again the developed numerical model simulates cerebral blood flow rate in a good agreement with the literature for the evaluated physiological scenarios within these arterial CO_2 pressure ($p_{a,CO2}$) and arterial O_2 pressure ($p_{a,O2}$) ranges. Uniqueness of the curve fitting was not evaluated in Eq. (2) which describes the O_2 cerebrovascular reactivity.

5. Conclusions

Numerical model developed in this study simulates cerebral blood flow rate within the physiological range for normophsyiology and studied physiological conditions. The developed numerical model can be used to evaluate different clinical and physiological scenarios which alter the cerebral blood flow rate.

CRediT authorship contribution statement

Selim Bozkurt: Conceptualization, Methodology, Software, Writing – original draft, Supervision. **A. Volkan Yilmaz:** Software, Writing – review & editing. **Kaushiki Bakaya:** Formal analysis, Writing – review & editing. **Aniket Bharadwaj:** Formal analysis, Writing – review & editing. **Koray K. Safak:** Supervision, Writing – review & editing.

Declaration of Competing Interest

The authors declare that they have no known competing financial interests or personal relationships that could have appeared to influence the work reported in this paper.

Appendix A. Supplementary data

Supplementary data to this article can be found online at https://doi.org/10.1016/j.bspc.2022.103851.

References

[1] E.C. Peterson Z. Wang G. Britz Regulation of Cerebral Blood Flow International Journal of Vascular Medicine. 2011 2011 1 8 e823525.

[2] M.J. Cipolla, Control of Cerebral Blood Flow, Morgan & Claypool Life Sciences, 2009. https://www.ncbi.nlm.nih.gov/books/NBK53082/ (accessed December 21, 2020).

[3] W.M. Armstead, Cerebral blood flow autoregulation and dysautoregulation, Anesthesiol Clin. 34 (2016) 465–477, https://doi.org/10.1016/j.anclin.2016.04.002.

[4] S.J. Payne, Cerebral blood flow and metabolism: A quantitative approach, World Scientific, 2017.

[5] E. Bor-Seng-Shu, W.S. Kita, E.G. Figueiredo, W.S. Paiva, E.T. Fonoff, M.J. Teixeira, R.B. Panerai, Cerebral hemodynamics: concepts of clinical importance, Arq. Neuropsiquiatr. 70 (2012) 352–356, https://doi.org/10.1590/S0004-282X2012000500010.

[6] W.K. Cornwell, A.V. Ambardekar, T. Tran, J.D. Pal, L. Cava, J. Lawley, T. Tarumi, C.L. Cornwell, K. Aaronson, Stroke incidence and impact of continuous-flow left ventricular assist devices on cerebrovascular physiology, Stroke 50 (2) (2019) 542–548.

[7] R. Sean, A. Venkatesh, Cerebral autoregulation and blood pressure lowering, Hypertension 49 (2007) 977–978, https://doi.org/10.1161/HYPERTENSIONAHA.107.087502.

[8] M. Ursino, A mathematical study of human intracranial hydrodynamics part 1—The cerebrospinal fluid pulse pressure, Ann. Biomed. Eng. 16 (1988) 379–401, https://doi.org/10.1007/BF02364625.

[9] S.K. Piechnik, P.A. Chiarelli, P. Jezzard, Modelling vascular reactivity to investigate the basis of the relationship between cerebral blood volume and flow under CO2 manipulation, Neuroimage. 39 (2008) 107–118, https://doi.org/10.1016/j.neuroimage.2007.08.022.

[10] M. Ursino, C.A. Lodi, A simple mathematical model of the interaction between intracranial pressure and cerebral hemodynamics, J. Appl. Physiol. 82 (1997) 1256–1269, https://doi.org/10.1152/jappl.1997.82.4.1256.

[11] M. Ursino, C.A. Lodi, Interaction among autoregulation, CO2 reactivity, and intracranial pressure: a mathematical model, Am. J. Physiol. 274 (1998) H1715–H1728, https://doi.org/10.1152/ajpheart.1998.274.5.H1715.

[12] M.C. Aoi, C.T. Kelley, V. Novak, M.S. Olufsen, Optimization of a mathematical model of cerebral autoregulation using patient data, IFAC Proceedings Volumes. 42 (2009) 181–186, https://doi.org/10.3182/20090812-3-DK-2006.0088.

[13] M. Banaji, I. Tachtsidis, D. Delpy, S. Baigent, A physiological model of cerebral blood flow control, Math. Biosci. 194 (2005) 125–173, https://doi.org/10.1016/j.mbs.2004.10.005.

[14] S.J. Payne, J. Selb, D.A. Boas, Effects of autoregulation and CO2 reactivity on cerebral oxygen transport, Ann. Biomed. Eng. 37 (2009) 2288–2298, https://doi.org/10.1007/s10439-009-9763-5.

[15] B. Spronck, E.G.H.J. Martens, E.D. Gommer, F.N. van de Vosse, A lumped parameter model of cerebral blood flow control combining cerebral autoregulation and neurovascular coupling, Am J Physiol Heart Circ Physiol. 303 (2012) H1143–H1153, https://doi.org/10.1152/ajpheart.00303.2012.

[16] A. Mahdi, M.S. Olufsen, S.J. Payne, Mathematical model of the interaction between baroreflex and cerebral autoregulation, ArXiv:1512.04573 [q-Bio]. (2015). http://arxiv.org/abs/1512.04573 (accessed January 20, 2022).

[17] M. Czosnyka, S. Piechnik, H.K. Richards, P. Kirkpatrick, P. Smielewski, J. D. Pickard, Contribution of mathematical modelling to the interpretation of bedside tests of cerebrovascular autoregulation, J. Neurol. Neurosurg. Psychiatry 63 (1997) 721–731, https://doi.org/10.1136/jnnp.63.6.721.

[18] S.K. Piechnik, M. Czosnyka, N.G. Harris, P.S. Minhas, J.D. Pickard, A model of the cerebral and cerebrospinal fluid circulations to examine asymmetry in cerebrovascular reactivity, J. Cereb. Blood Flow Metab. 21 (2001) 182–192, https://doi.org/10.1097/00004647-200102000-00010.

[19] J. Duffin, G.M.T. Hare, J.A. Fisher, A mathematical model of cerebral blood flow control in anaemia and hypoxia, The Journal of Physiology. 598 (2020) 717–730, https://doi.org/10.1113/JP279237.

[20] X. Liu, M. Czosnyka, J. Donnelly, D. Cardim, M. Cabeleira, D.A. Lalou, X. Hu, P. J. Hutchinson, P. Smielewski, Assessment of cerebral autoregulation indices – a modelling perspective, Sci. Rep. 10 (2020) 9600, https://doi.org/10.1038/s41598-020-66346-6.

[21] S. Bozkurt, Effect of cerebral flow autoregulation function on cerebral flow rate under continuous flow left ventricular assist device support, Artif. Organs 42 (2018) 800–813, https://doi.org/10.1111/aor.13148.

[22] R.B. Panerai, Cerebral autoregulation: from models to clinical applications, Cardiovasc. Eng. 8 (2008) 42–59, https://doi.org/10.1007/s10558-007-9044-6.

[23] M. Ursino, M. Giannessi, A model of cerebrovascular reactivity including the circle of willis and cortical anastomoses, Ann. Biomed. Eng. 38 (2010) 955–974, https://doi.org/10.1007/s10439-010-9923-7.

[24] P.N. Ainslie, J. Duffin, Integration of cerebrovascular CO2 reactivity and chemoreflex control of breathing: mechanisms of regulation, measurement, and interpretation, Am. J. Physiol.-Regulatory, Integrative and Comparative Physiology. 296 (2009) R1473–R1495, https://doi.org/10.1152/ajpregu.91008.2008.

[25] M. Reivich, Arterial PCO2 and cerebral hemodynamics, Am. J. Physiol. 206 (1964) 25–35, https://doi.org/10.1152/ajplegacy.1964.206.1.25.

[26] A.M. Harper, H.I. Glass, Effect of alterations in the arterial carbon dioxide tension on the blood flow through the cerebral cortex at normal and low arterial blood pressures, J. Neurol. Neurosurg. Psychiatry 28 (1965) 449–452, https://doi.org/10.1136/jnnp.28.5.449.

[27] P. Das, A. Luoma, Applied cerebral physiology, Anaesthesia & Intensive Care Medicine. 21 (2020) 45–50, https://doi.org/10.1016/j.mpaic.2019.10.012.

[28] R.J. Traystman, Chapter 11 - cerebral blood flow regulation (carbon dioxide, oxygen, and nitric oxide), in: L.R. Caplan, J. Biller, M.C. Leary, E.H. Lo, A. J. Thomas, M. Yenari, J.H. Zhang (Eds.), Primer on Cerebrovascular Diseases (Second Edition), Academic Press, San Diego, 2017, pp. 60–67, https://doi.org/10.1016/B978-0-12-803058-5.00011-4.

[29] J.E. Hall Guyton and Hall Textbook of Medical Physiology 13th edition 2015 Saunders Philadelphia, PA.

[30] T. Korakianitis, Y. Shi, A concentrated parameter model for the human cardiovascular system including heart valve dynamics and atrioventricular interaction, Med. Eng. Phys. 28 (2006) 613–628, https://doi.org/10.1016/j.medengphy.2005.10.004.

[31] S. Bozkurt, E.G. Tolkacheva, Mathematical modeling of cardiac function to evaluate clinical cases in adults and children, PLoS ONE 14 (10) (2019) e0224663.

[32] L. Zarrinkoob, K. Ambarki, A. Wåhlin, R. Birgander, A. Eklund, J. Malm, Blood flow distribution in cerebral arteries, J. Cereb. Blood Flow Metab. 35 (2015) 648–654, https://doi.org/10.1038/jcbfm.2014.241.

[33] B.W. Smith, S. Andreassen, G.M. Shaw, P.L. Jensen, S.E. Rees, J.G. Chase, Simulation of cardiovascular system diseases by including the autonomic nervous system into a minimal model, Comput. Methods Programs Biomed. 86 (2007) 153–160, https://doi.org/10.1016/j.cmpb.2007.02.001.

[34] Z. Messina, H. Patrick, Partial Pressure of Carbon Dioxide, in: StatPearls, StatPearls Publishing, Treasure Island (FL), 2022. http://www.ncbi.nlm.nih.gov/books/NBK551648/ (accessed May 14, 2022).

[35] S. Sharma, M.F. Hashmi, Partial Pressure Of Oxygen, in: StatPearls, StatPearls Publishing, Treasure Island (FL), 2022. http://www.ncbi.nlm.nih.gov/books/NBK493219/ (accessed May 14, 2022).

[36] T.G. Papaioannou, A.D. Protogerou, D. Vrachatis, G. Konstantonis, E. Aissopou, A. Argyris, E. Nasothimiou, E.J. Gialafos, M. Karamanou, D. Tousoulis, P. P. Sfikakis, Mean arterial pressure values calculated using seven different methods and their associations with target organ deterioration in a single-center study of 1878 individuals, Hypertens. Res. 39 (2016) (1878) 640–647, https://doi.org/10.1038/hr.2016.41.

[37] T. Lepic, G. Loncar, B. Bozic, D. Veljancic, B. Labovic, Z. Krsmanovic, M. Lepic, R. Raicevic, Cerebral blood flow in the chronic heart failure patients, Perspectives in Medicine. 1 (2012) 304–308, https://doi.org/10.1016/j.permed.2012.02.057.

[38] P.J. Eames, M.J. Blake, S.L. Dawson, R.B. Panerai, J.F. Potter, Dynamic cerebral autoregulation and beat to beat blood pressure control are impaired in acute ischaemic stroke, J. Neurol. Neurosurg. Psychiatry 72 (2002) 467–472, https://doi.org/10.1136/jnnp.72.4.467.

[39] F.A. Zeiler, A. Ercole, M. Czosnyka, P. Smielewski, G. Hawryluk, P.J.A. Hutchinson, D.K. Menon, M. Aries, Continuous cerebrovascular reactivity monitoring in moderate/severe traumatic brain injury: a narrative review of advances in neurocritical care, Br. J. Anaesth. 124 (2020) 440–453, https://doi.org/10.1016/j.bja.2019.11.031.

[40] K. Møller, F.S. Larsen, J. Qvist, J.H. Wandall, G.M. Knudsen, I.E. Gjørup, P. Skinhøj, Dependency of cerebral blood flow on mean arterial pressure in patients with acute bacterial meningitis, Crit. Care Med. 28 (4) (2000) 1027–1032.

[41] R.V. Immink, B.-J.-H. van den Born, G.A. van Montfrans, R.P. Koopmans, J. M. Karemaker, J.J. van Lieshout, Impaired Cerebral Autoregulation in Patients With Malignant Hypertension, Circulation 110 (2004) 2241–2245, https://doi.org/10.1161/01.CIR.0000144472.08647.40.
[42] S. Patel, J.H. Miao, E. Yetiskul, A. Anokhin, S.H. Majmundar, Physiology, Carbon Dioxide Retention, in: StatPearls, StatPearls Publishing, Treasure Island (FL), 2021. http://www.ncbi.nlm.nih.gov/books/NBK482456/ (accessed January 2, 2022).
[43] S. Sharma, M.F. Hashmi, Hypocarbia, in: StatPearls, StatPearls Publishing, Treasure Island (FL), 2021. http://www.ncbi.nlm.nih.gov/books/NBK493167/ (accessed January 2, 2022).
[44] J. Marhong, E. Fan, Carbon dioxide in the critically Ill: too much or too little of a good thing? Respiratory Care. 59 (2014) 1597–1605, https://doi.org/10.4187/respcare.03405.
[45] M. Sarkar, N. Niranjan, P. Banyal, Mechanisms of hypoxemia, Lung India. 34 (2017) 47–60, https://doi.org/10.4103/0970-2113.197116.
[46] A.J. Johnston, L.A. Steiner, A.K. Gupta, D.K. Menon, Cerebral oxygen vasoreactivity and cerebral tissue oxygen reactivity, Br. J. Anaesth. 90 (2003) 774–786, https://doi.org/10.1093/bja/aeg104.
[47] R.L. Hoiland, A.R. Bain, M.G. Rieger, D.M. Bailey, P.N. Ainslie, Hypoxemia, oxygen content, and the regulation of cerebral blood flow, American Journal of Physiology-Regulatory, Integrative and Comparative Physiology. 310 (2016) R398–R413, https://doi.org/10.1152/ajpregu.00270.2015.
[48] F.P. Tiecks, A.M. Lam, R. Aaslid, D.W. Newell, Comparison of static and dynamic cerebral autoregulation measurements, Stroke 26 (1995) 1014–1019, https://doi.org/10.1161/01.STR.26.6.1014.
[49] M. Czosnyka, N.G. Harris, J.D. Pickard, S. Piechnik, CO2 cerebrovascular reactivity as a function of perfusion pressure — a modelling study, Acta Neurochir. 121 (1993) 159–165, https://doi.org/10.1007/BF01809269.
[50] C. Wu, A.R. Honarmand, S. Schnell, R. Kuhn, S.E. Schoeneman, S.A. Ansari, J. Carr, M. Markl, A. Shaibani, Age-related changes of normal cerebral and cardiac blood flow in children and adults aged 7 months to 61 years, J Am Heart Assoc. 5 (2016) e002657.
[51] J. Ledoux, D.M. Gee, N. Leblanc, Increased peripheral resistance in heart failure: new evidence suggests an alteration in vascular smooth muscle function, Br. J. Pharmacol. 139 (2003) 1245–1248, https://doi.org/10.1038/sj.bjp.0705366.
[52] M. Naranjo, M. Paul, Malignant Hypertension, in: StatPearls, StatPearls Publishing, Treasure Island (FL), 2021. http://www.ncbi.nlm.nih.gov/books/NBK507701/ (accessed January 8, 2022).
[53] J.M. Pollock, A.R. Deibler, C.T. Whitlow, H. Tan, R.A. Kraft, J.H. Burdette, J. A. Maldjian, Hypercapnia-induced cerebral hyperperfusion: an underrecognized clinical entity, American Journal of Neuroradiology. 30 (2009) 378–385, https://doi.org/10.3174/ajnr.A1316.
[54] C.L. Jarrett, K.L. Shields, R.M. Broxterman, J.R. Hydren, S.H. Park, J.R. Gifford, R. S. Richardson, Imaging transcranial Doppler ultrasound to measure middle cerebral artery blood flow: the importance of measuring vessel diameter, American Journal of Physiology-Regulatory, Integrative and Comparative Physiology. 319 (2020) R33–R42, https://doi.org/10.1152/ajpregu.00025.2020.
[55] M.D. Ford, N. Alperin, S.H. Lee, D.W. Holdsworth, D.A. Steinman, Characterization of volumetric flow rate waveforms in the normal internal carotid and vertebral arteries, Physiol. Meas. 26 (2005) 477–488, https://doi.org/10.1088/0967-3334/26/4/013.
[56] D.P. Zipes, P. Libby, R.O. Bonow, D.L. Mann, G.F. Tomaselli, E. Braunwald, Braunwald's heart disease: a textbook of cardiovascular medicine., Eleventh edition / edited by Douglas P. Zipes, MD, Peter Libby, MD, Robert O. Bonow, MD, Douglas L. Mann, MD, Gordon F. Tomaselli, MD ; founding editor and online editor, Eugene Braunwald, MD, MD(Hon), ScD(Hon), FRCP., Elsevier, Philadelphia, PA, 2019.
[57] N. Gruhn, F.S. Larsen, S. Boesgaard, G.M. Knudsen, S.A. Mortensen, G. Thomsen, J. Aldershvile, Cerebral blood flow in patients with chronic heart failure before and after heart transplantation, Stroke 32 (2001) 2530–2533, https://doi.org/10.1161/hs1101.098360.
[58] N.S. Coverdale, S. Lalande, A. Perrotta, J.K. Shoemaker, Heterogeneous patterns of vasoreactivity in the middle cerebral and internal carotid arteries, Am J Physiol Heart Circ Physiol. 308 (2015) H1030–H1038, https://doi.org/10.1152/ajpheart.00761.2014.
[59] H. Ito, I. Kanno, M. Ibaraki, J. Hatazawa, S. Miura, Changes in human cerebral blood flow and cerebral blood volume during hypercapnia and hypocapnia measured by positron emission tomography, J. Cereb. Blood Flow Metab. 23 (2003) 665–670, https://doi.org/10.1097/01.WCB.0000067721.64998.F5.
[60] K.J. Smith, P.N. Ainslie, Regulation of cerebral blood flow and metabolism during exercise, Exp. Physiol. 102 (2017) 1356–1371, https://doi.org/10.1113/EP086249.
[61] S. Ogoh, G. Moralez, T. Washio, S. Sarma, M. Hieda, S.A. Romero, M.N. Cramer, M. Shibasaki, C.G. Crandall, Effect of increases in cardiac contractility on cerebral blood flow in humans, Am J Physiol Heart Circ Physiol. 313 (2017) H1155–H1161, https://doi.org/10.1152/ajpheart.00287.2017.
[62] P. Brassard, L. Labrecque, J.D. Smirl, M.M. Tymko, H.G. Caldwell, R.L. Hoiland, S. J.E. Lucas, A.Y. Denault, E.J. Couture, P.N. Ainslie, Losing the dogmatic view of cerebral autoregulation, Physiol Rep. 9 (2021) e14982. https://doi.org/10.14814/phy2.14982.